Nanoscale

PAPER

View Article Online
View Journal | View Issue

Cite this: *Nanoscale*, 2025, **17**, 25589

Occupational exposure to graphene-related materials: from workplace emissions to health risk assessment

Mikko Poikkimäki, *[a] Jussi Lyyränen,[a] Arman Ilyas,[a] Kukka Aimonen,[a] Pasi Huuskonen, [a] Maija Leppänen, [a] Jonna Weisell-Laitinen, [a] Julio Gómez [b] and Tomi Kanerva [a]

Graphene-related materials (GRMs) are among the most promising and versatile advanced materials, offering a wide range of applications. However, concerns regarding occupational exposure and associated safety challenges remain critical in their development and use. This study assessed exposures to GRMs, including graphene, graphene oxide (GO), reduced graphene oxide (rGO), and few-layer graphene (FLG), across seven real-world and three simulated exposure scenarios. Airborne GRM exposures in production, processing, and handling environments were measured and characterised using a standardised, tiered approach. Emissions were further evaluated through number-based dustiness testing of five GRMs (three rGOs, one GO, and one FLG), with the resulting dustiness data supporting exposure and lung deposition modelling. A health risk assessment was performed using both measured and modelled exposures. Workplace studies indicated low exposure during GRM production and related activities, primarily due to effective safety measures and practices. GRMs were typically processed in small quantities, in liquid form, or within closed systems, resulting in low exposure potential. Consequently, the risk to workers remained low, particularly with consistent use of personal protective equipment. However, handling GRMs as dry powders or in larger volumes may increase emissions, leading to higher exposures and potential health risks. Special attention is warranted during scale-up or process changes to prevent GRM emissions and exposures. Worker safety can be maintained by adapting traditional occupational hygiene practices to nanomaterial-specific considerations; nevertheless, a precautionary approach is recommended given prevailing uncertainties regarding long-term health effects.

Received 8th May 2025,
Accepted 29th September 2025
DOI: 10.1039/d5nr01885d
rsc.li/nanoscale

Introduction

Graphene-related materials (GRMs) are a large family of two-dimensional, carbon-based materials with diverse physicochemical characteristics, including variable lateral size, thickness, surface area, shape, carbon-to-oxygen (C/O) ratio, and surface chemistry.[1,2] The physicochemical properties of GRMs guide their interaction with biological systems, which may affect their hazard potential and possible toxic responses.

The hazard properties of GRMs have been reviewed extensively.[2–11] Studies have documented lung inflammation[12–14] and the onset of lung fibrosis following pulmonary exposure to graphene oxide (GO)[15] and graphene nanoplatelets (GNPs).[16] Notably, pulmonary effects have been linked to the distinct physicochemical properties of GO, such as a lateral size exceeding several microns.[14,17–19] Despite their large lateral size, GRMs are respirable due to unique aerodynamic properties. It is hypothesised that deposition of laterally large particles deep in the lungs drives inflammation.[20] Some GRMs may also have genotoxic and carcinogenic properties,[2] which may result from oxidative stress and production of reactive oxygen species.[21,22] While GO is generally found to be more toxic than reduced graphene oxide (rGO),[13,23] rGO has also shown adverse health effects, such as macrophage-driven granulomatosis.[24]

The primary risk of GRMs to human health is associated with inhalation exposure during production, use, and waste disposal.[25,26] Therefore, understanding workplace exposures and the airborne emission potential of GRMs is essential for developing effective occupational safety strategies.

Exposures to airborne particles have been reported in many GRM workplaces. Heitbrink *et al.*[27] measured particle releases during the cleaning of a process tank and the collection of GNP powder into containers. Subsequently, Spinazzè *et al.*

[a]*Finnish Institute of Occupational Health, P.O. Box 40, FI-00032 Työterveyslaitos, Helsinki, Finland. E-mail: mikko.poikkimaki@ttl.fi*
[b]*Avanzare Innovación Tecnológica S.L., Av. Lentiscares 4-6, 26370 Navarrete, Spain*

found elevated particle concentrations during graphene production[28] and GNP handling.[29] However, no data on the composition of the particles were reported, leaving open the question of whether graphene is emitted into the workplace air.

Boccuni *et al.*[30] identified a brief (1-minute) release of nanoparticles during graphite spraying in a laboratory-scale graphene manufacturing, but did not indicate the presence of graphene. Similar observations were made in graphene manufacturing utilising chemical vapour deposition (CVD).[31] In a GNP production (graphite exfoliation and CVD),[32] the particle number concentration (PNC) increased, and black carbon was found in workplace air, with no indication of graphene.

Exposure to GNPs was further studied at a laboratory scale through thermal expansion of graphite flakes, followed by liquid exfoliation.[33] The PNC increased during the process, indicating a risk of exposure. However, only an intermediate product (worm-like expanded graphite), not graphene, was identified in air samples. Furthermore, during the production of nanocomposite paint, including tip-sonication and spray coating with GNPs,[34] short increases in PNC and average diameter were observed during furnace opening and spray coating, indicating a release of larger particles. The particles were confirmed to be carbon-based and had a morphology similar to that of the produced GNPs.

The occupational exposure potential was also studied in a pilot-scale manufacturing process for rGO, including chemical oxidation of graphite and thermal reduction of GO in a tubular oven.[35] High PNCs were observed but were attributed to ambient and engine-generated nanoparticles rather than rGO or intermediates, although a few agglomerates of rGO consisting of micron-sized flakes were identified in workplace air.

Beyond GRM manufacturing, industrial handling of powdered GRMs poses a risk of exposure. Lovén *et al.*[36] observed significant but brief (1-minute) releases during weighing and mixing of dry GNPs and GO powders. Elemental carbon (EC) concentration, an indicator of graphene, increased at the GO source (1.9 μg m^{-3}) and in the worker's breathing zone (BZ, 1.3 μg m^{-3}) due to an open process. However, GNPs (EC = 26 μg m^{-3}) did not transfer from the fume hood to the BZ. Higher EC exposures (20–60 μg m^{-3}) have been reported during other GRM powder handling.[37]

Fito López *et al.*[38] found individual aerosol particles with GO-like morphology and chemical composition in the near-field of laboratory-scale GO synthesis. They also detected a brief 3-minute PNC peak (max. 1.4×10^5 cm^{-3}) during weighing and transferring of dry powdered rGO, likely originating from the process, but no identification of particle morphology or chemical composition was reported. Apart from dry-powder handling, free submicron GRMs, especially GO and rGO, can be released from epoxy composites when abraded.[39]

The exposure to few-layer graphene (FLG) has been extensively studied in a graphene-producing plant, including liquid-phase exfoliation of graphite (wet-jet milling), rotary evaporation (liquid), freeze-drying (powder), and storing and cleaning (powder). FLG production resulted in a higher PNC at the BZ than background.[40] The highest values were measured during wet-jet milling, during which a release of volatile organic compounds was also observed. Thus, the exposure might not be exclusively attributed to FLG. However, the risk of exposure to FLG itself was present during storage and cleaning, during which it was handled in powder form. In a following study,[41] nanoparticles were found in the worker's BZ, indicating possible FLG release, especially during handling of FLG in a dry powder form (drying and storing phases). After upscaling production from pilot (100 g) to industrial-scale (2 kg), the FLG exposure potential was revisited,[42] demonstrating the effectiveness of closed systems in mitigating exposure. However, an open FLG powder-handling phase showed increased exposure potential, with a PNC of 3500 cm^{-3} and a submicron particulate mass (PM_1) of 3 μg m^{-3} above background levels.

Despite excellent efforts demonstrating GRM dust releases into workplace air, especially during handling dry GRM powders, the airborne emission rates remain to be quantified. The emission rates of powdered materials, such as many GRMs, can be determined, for example, by dustiness tests simulating workplace processes in a controlled environment. Dustiness describes a material's ability to generate airborne particles during handling.[43] It provides comparable data on the emission potential of different materials. It is applicable, for example, to exposure assessment and modelling,[44–46] and ultimately to selecting less dusty GRMs for production and use.

To date, dustiness data for various nanomaterials have been reported, for example, for carbon nanotubes,[47] but they are lacking for GRMs. We report the first-ever number-based dustiness indices and emissions rates for five GRMs (three rGOs, a GO, and a FLG), along with detailed characterisation of aerosol size distributions, chemical composition, and morphology. The dustiness data are further utilised for exposure assessment.

Occupational exposure to various GRMs is assessed across ten exposure scenarios, encompassing novel experiments conducted in real-world manufacturing and handling facilities, as well as modelling of worst-case exposures in future industrial scenarios with increased production volumes. The assessment combines particle size and concentration estimates to a comprehensive chemical and morphological characterisation. Based on these results, lung deposition modelling and graphene-related health risk assessments are conducted. Finally, guidance and recommendations for safe GRM work are presented.

Materials and methods

Graphene-related materials

GRM powders tested in this study included three reduced graphene oxide variants, one graphene oxide, and one few-layer graphene. Powder-form rGOs, namely rGO1 and rGO2 (average lateral sizes: 2.4 μm and 1.9 μm, determined in culture media; C/O ratios: 52.6 and 7.1), were prepared by thermochemical reduction of GO, as described previously by Rodriguez-Garraus *et al.*[48] (referred to as rGO1 and rGO4 therein). GO (average lateral size: 2.5 ± 2.3 μm; C/O ratio: 1.2) was synthesised using a modified Hummers' method (patent EP 3070053B1), while rGO3 (average lateral size: 3.2 ± 1.8 μm; C/O ratio 5.3) was prepared *via* ascorbic acid reduction of GO (patent WO 2019145378A1), as detailed by Pelin *et al.*[49] (where it is termed rGO). FLG (lateral size range: 0.1–1 μm) was synthesised by wet-jet milling exfoliation, followed by rotary evaporation and freeze-drying, as reported by Tombolini *et al.*[41]

Aerosol sampling and analysis

Airborne GRMs were studied using multiple metrics. Particle number concentration (PNC) was measured with an ultrafine condensation particle counter (UCPC 3776, TSI Inc.), which has a detection limit of 2.5 nm. PNC, lung deposited surface area (LDSA), and average particle size were measured using a handheld diffusion charger (DISCmini, Testo SE & Co. KGaA), equipped with a pre-impactor (10–700 nm).[50] Number size distributions (6 nm–10 μm) were obtained using electrical low-pressure impactors (ELPI[51] and ELPI+,[52] Dekati Ltd).

For chemical composition and morphology analysis, particles were collected on holey carbon film, 200 mesh Cu grids (Agar Scientific Ltd), using a mini particle sampler (MPS, Ecomesure SAS) with a flow rate of 0.3 L min^{-1} (Gilian GilAir Plus, Sensidyne). Additional samples were collected using an in-house method[53] for high-volume sampling (10 L min^{-1}). The samples were analysed with a JEOL JEM-1400 Flash transmission electron microscope (TEM) equipped with a JEOL Dry SD30GV energy dispersive X-ray (EDX) detector, operated at 80 kV. To ensure statistical reliability, 252 (for 0.02–0.55 μm) and 118 (for 0.55–40 μm) individual particles were counted. The particle size and aspect ratio were determined by fitting particles inside a rectangle to define the main axis dimensions. The counted size distributions were corrected for the collection efficiency of the MPS sampler.[54,55]

Elemental carbon (EC) content of the particles was determined by collecting the aerosol on 25 mm quartz fibre filters (SKC Ltd) loaded into styrene cassettes (clear, 3-piece, SKC Ltd) at a flow rate of 2.75 L min^{-1} (Gilian 5000, Sensidyne). The filters were analysed thermal-optically with an organic and elemental carbon analyser, model 5L (Sunset Laboratory Inc.). The method is based on the NIOSH 5040 standard,[56–58] with a limit of quantification (LOQ) of 0.31 μg cm^{-2}, and has been recommended previously[37] for GRM exposure measurements. A respirable dust cyclone was utilised for EC sampling in the dustiness testing (FSP10, GSA Messgerätebau GmbH, 10 L min^{-1}) and the workplace measurements (GS-1, SKC Ltd).

Dustiness testing

Five GRMs (rGO1, rGO2, rGO3, GO, FLG) were tested according to the European standard for dustiness testing of materials containing nano-objects and their agglomerates and aggregates,[59] using the rotating drum method.[60] The results were used to calculate number-based dustiness indexes (DI) and emission rates for the tested GRMs. For each material, the dustiness test was replicated at least three times with identical samples (17.5 ± 0.5 mL), according to the standard's requirements. The tests were conducted in a temperature- and humidity-controlled room and monitored using a VelociCalc/Q-Trak (model 7565/9555-P, TSI Inc.).

Workplace measurements

Occupational exposure to potentially released GRM particles in the air was assessed during graphene-related work operations in accordance with CEN standards.[61,62] A total of seven different exposure scenarios were evaluated in five workplaces. Two of the workplaces were commercial companies producing GRMs, while the other three were research institute laboratories conducting GRM work at laboratory and pilot scale.

Exposure measurements (Tier 1–3) were carried out as activity-based (static) in selected locations in the near-field (NF), far-field (FF), and background (BG) areas, as well as breathing zone (BZ) measurements of the worker (mobile). The exposure scenarios, measurement locations and sampling devices are detailed in Table S1. The study focused on detecting possible GRM particle emissions from the processes and measuring exposure potential. In the interpretation of the results, the BG particle concentration resulting from other emission sources or outdoor air was distinguished from process-related particles. The BG was measured simultaneously with an identical DISCmini device in a location not affected by the process emissions, and the BG for ELPI+ was collected before the process start. A significant exposure concentration was defined as background plus three times the standard deviation (BG + $3{\cdot}\sigma_{BG}$) as per the measurement standard.[62] EC sampling from workplace air, together with TEM sample collection, was combined with airborne PNC measurements, providing further information about the presence of GRMs in workplace air.

Exposure model

In addition to workplace measurements, three scenarios were generated to predict future GRM use in laboratory, pilot, and industrial-scale operations; see Table S2. The laboratory-scale tasks used a similar amount of GRM as in dustiness testing (17.5 mL), with the pilot-scale being 10-fold and the industrial-scale assumed to be 100-fold. GRM release rates were based on the simulated work operations (see Dustiness testing). A constant particle emission, S, was considered to emit GRM to the workplace air for t_{emis} = 30 minutes:

$$S = \mathrm{DI} \times \frac{\mathrm{d}m}{\mathrm{d}t}, \tag{1}$$

where DI is the dustiness index of the material in mg^{-1} and dm/dt is the mass flow of the material (mg min^{-1}) in the process.

The PNCs at the worker BZ were calculated with a turbulent diffusion model according to Poikkimäki *et al.*[63] The PNC was modelled at the location (x, y, z) over time t by

$$\mathrm{PNC}(x,y,z,t)=\int_0^{t_{\mathrm{emis}}}\frac{S}{(4\pi Kt)^{\frac{3}{2}}}\exp\left(-at+\frac{w_{\mathrm{d}}A}{V}t\right)R_xR_yR_z\mathrm{d}t, \quad (2)$$

where K ($\mathrm{m}^2\ \mathrm{s}^{-1}$) is the turbulent diffusion coefficient, a (s^{-1}) is the ventilation rate, w_{d} ($\mathrm{m\ s}^{-1}$) is the deposition rate, A (m^2) is the deposition surface area, V (m^3) is the room volume, and R_x (x), R_y (y), and R_z (y) are the wall reflection terms.[63,64] The maximum PNC at $t = t_{\mathrm{emis}}$ was assumed as the worst-case exposure.

Modelled number size distributions were attained by normalising the measured distributions (see Dustiness testing) in the submicron size range (ELPI stages, i = 1–8) by modelled total PNCs. The resulting distributions were then converted to mass distributions assuming spherical particles with aerodynamic diameters of $d_{\mathrm{p},i}$, and material bulk densities ρ_{GRM} determined for each material, following the equation:

$$\frac{\mathrm{d}M}{\mathrm{d}\log d_{\mathrm{p},i}}=\frac{\pi\cdot\rho_{\mathrm{GRM}}}{6}{d_{\mathrm{p},i}}^3\frac{\mathrm{d}N}{\mathrm{d}\log d_{\mathrm{p},i}}. \quad (3)$$

Lognormal distributions were then fitted to obtain mass median aerodynamic diameter (MMAD), geometric standard deviation (GSD), and mass fraction of each mode, to be used for subsequent lung deposition modelling.

Lung deposition model

The lung deposition of the studied GRMs was modelled in human and rat respiratory tracts using the Multiple-Path Particle Dosimetry (MPPD) model (version 3.04, Applied Research Associates). A human nasal breather was assumed, performing light exercise (breathing frequency of 19 per minute and tidal volume of 1000 mL) in an upright body orientation, similar to earlier work by Lee *et al.*[65] For airway morphometry, the Yeh/Schum 5-lobe lung model was employed, assuming both lung deposition and clearance with MPPD default values. Exposure data were obtained from the workplace measurements and exposure modelling. In each scenario, graphene-related work was assumed to be repeated for 30 min day^{-1}, 5 days per week, for 18 weeks. Lung deposition in rats was modelled similarly to Lee *et al.*[65]

Health risk assessment

To assess potential health effects caused by the studied GRMs, literature data[65–72] on the inhalation toxicity of experimental animals (rats) was surveyed to identify the no-observed-adverse-effect concentrations (NOAECs). The lowest NOAEC (0.5 mg m^{-3}) across studies was used to calculate the human equivalent concentration (HEC), indicating similar effects in humans. HECs were calculated for the studied GRMs using the methodology reported by Lee *et al.*,[65] assuming the alveolar deposition fractions modelled in this study.

In the absence of official occupational exposure limits (OELs) for GRMs, we compared the measured and modelled exposure concentrations with HECs and further calculated a risk characterisation ratio (RCR) for each GRM. An RCR value, defined as the exposure concentration divided by the HEC, greater than unity, indicates an increased health risk.[73]

As a further comparison point, we utilised the health-based guidance values (GVs) of 0.212 mg m^{-3} and $9.37\times10^4\ \mathrm{cm}^{-3}$ determined for inhalation exposure to GNPs,[74] and the derived no-effect levels (DNELs) of 0.063 and 0.101 μg m^{-3} for graphene and GO,[75] based on ECHA guidance (Chapter R.8). In addition, we adopted a generic nano reference value of 40 000 cm^{-3}, as an 8-hour time-weighted average ($\mathrm{NRV_{8h}}$) proposed for nanoparticles with a density lower than 6 g cm^{-3}. For short exposures, an $\mathrm{NRV_{15min}}$ was defined as twice the $\mathrm{NRV_{8h}}$.[76]

Results and discussion

Dustiness testing

Three rGO variants, one GO, and one FLG were tested for dustiness. The test was repeated for each material using multiple identical samples (Table 1). The dustiness indices, determined individually for each replicated sample, were uniform, except for a few outliers (Fig. 1). All rGO materials exhibited considerably higher number-based dustiness indices than GO and FLG, which is consistent with the indices calculated from respirable EC collection. Visual observations supported these results, showing that the rGO powders were extremely light

Table 1 Average number-based dustiness indices (DI_m) for graphene-related material (GRM) powders (reduced graphene oxide (rGO), graphene oxide (GO), and few-layer graphene (FLG)), including average sample volumes, masses (m), moisture contents, and bulk densities (ρ_{GRM}) with standard deviations (±)

	rGO1	rGO2	rGO3	GO	FLG
Replicates n	8	6	6	4	3
Volume (mL)	17.5	17.5	17.5	17.5	17.5
m (mg)	81 ± 8	79 ± 6	1131 ± 40	3536 ± 18	1685 ± 101
ρ_{GRM} (kg m^{-3})	4.6 ± 0.5	4.5 ± 0.4	65 ± 3	202 ± 2	96 ± 6
Moisture (%)	n/a[a]	n/a[a]	2.4 ± 0.1	4.1 ± 0.2	0.2 ± 0.005
DI_m (mg^{-1})	$2.0\pm0.5\times10^5$	$3.1\pm0.2\times10^5$	$3.4\pm0.3\times10^5$	$5.9\pm1.8\times10^3$	$3.4\pm0.3\times10^4$
DI_ν (–)	1.6×10^7	2.4×10^7	3.8×10^8	2.1×10^7	5.7×10^7
$\mathrm{DI_{EC}}$ (μg mg^{-1})	2.3	0.71	n/a	0.03	0.11

Dustiness indices per 17.5 mL of GRM powder are also reported as $\mathrm{DI}_\nu = \mathrm{DI}_m\cdot m$, along with the dustiness index of respirable elemental carbon ($\mathrm{DI_{EC}}$), expressed as EC mass emitted per sample mass (m). n/a = not available. [a] Determined moisture content close to zero but negative.

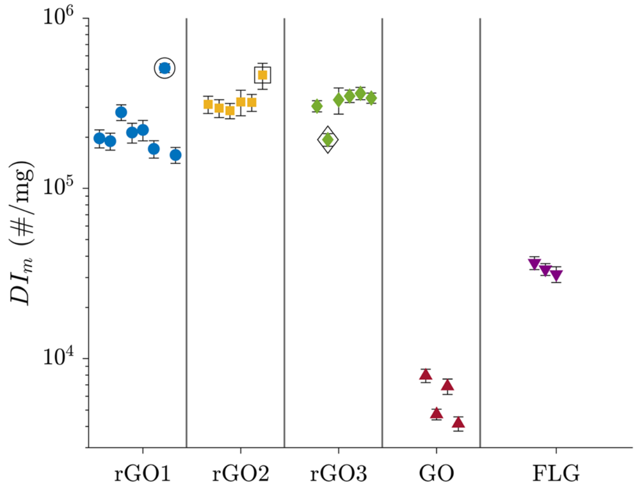

Fig. 1 Number-based dustiness indices for five GRMs from individual dustiness tests (n = 27), based on UCPC data (d_p = 2.5 nm–1 μm). Error bars indicate the limits from the propagation of uncertainty (maximal error). Outliers, encircled on the plot, likely result from measurement inconsistencies, such as partial clogging of sampling lines or the cyclone with GRM, affecting sampling flows or releasing GRM.

(low bulk density) and easily suspended in the surrounding air when handled.

A higher index can lead to increased workplace exposure during actions such as cleaning, scooping, and transferring powdered materials.[77] Therefore, increased attention to worker exposure mitigation measures is required during the production and handling of rGO materials.

No dustiness indices for GRMs are available in the literature for comparison with our results. However, Dazon *et al.*[47] measured number-based dustiness indices for 14 carbon nanotubes, which showed similar results ranging from 10^3 to 4 × 10^5 mg^{-1}, to those observed in this study for GRMs. Studies on other nanomaterials have reported wide variability, with values ranging from 10^4–10^5 and 10^6–10^9 particles per mg.[78,79]

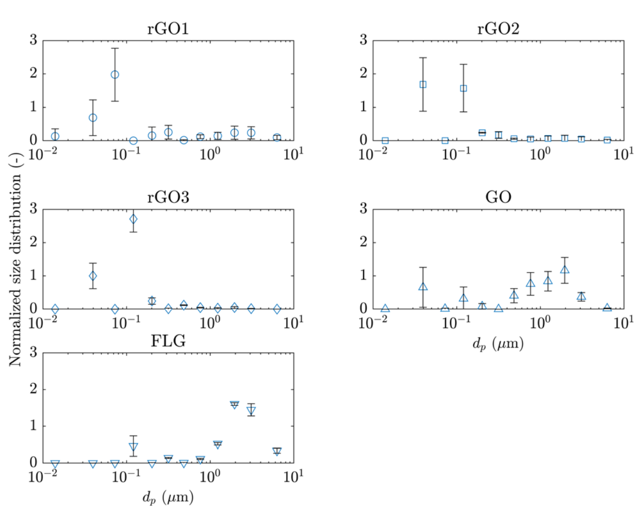

Fig. 2 Normalised number size distributions $f_n(d_{p,i})$, for dustiness-tested GRMs, showing the mean and standard deviation for each ELPI stage.[60] Data points near 0.07 μm for rGO2, rGO3, and GO are suspected outliers, likely due to a single ELPI stage becoming filled or clogged with GRM.

The particle number size distributions (Fig. 2) show that the aerosol comprises both nanometre- and micrometre-scale particles, indicating that GRM powders release particles across a broad size range. rGO powders emit more nanoparticles (<100 nm), while GO emits a similar order of magnitude, and FLG releases even more super-micron (>1 μm) than nanosized particles. This explains the large differences in dustiness indices between rGO, GO, and FLG materials, as the measurement of number-based dustiness index is limited to submicron particles (calculated from UCPC data). Materials that emit smaller nanoparticles are expected to have higher number-based dustiness indexes than those emitting larger particles.

Note also that the number-based dustiness indices (DI_m), as defined by the measurement standard,[60] are calculated per mg of GRM powder. Bulk densities of the powders varied by several orders of magnitude (0.0045–0.202 g cm^{-3}), resulting in indices per volume (DI_v) that are more similar between GRMs (Table 1). rGO1 and rGO2 have extremely low densities, combined with high specific surface areas (654 and 598 m^2 g^{-1}),[48] leading to high dustiness per mg. GO, which has a high density, shows low dustiness per mg, but its dustiness per volume is comparable to that of the other GRMs. Only rGO3 stands out, combining both high dustiness per mg and high density. Thus, whether a constant mass or volume of GRM powder is used in industrial applications significantly affects the emission potential. To improve comparability between materials,[79] we used dustiness indices (emission rates) per constant volume of 17.5 mL as the basis for exposure modelling in this study.

TEM analyses supported the dustiness index results: the highest concentrations on TEM samples correlated with high indices. The TEM images revealed leaflet-like particles ranging from nano- to super-micron sizes, and EDX analysis confirmed they were carbon-based. The rGO materials (Fig. 3A–C and Fig. S1–S5) showed super-micron particles together with near-spherical nanoparticles, while GO and FLG (Fig. 3D–E and Fig. S6–S8) consisted mainly of super-micron particles with fine sub-micron and nanoscale structures. These observations align with the number size distribution data (Fig. 2). However, it should be noted that the ELPI classifies particles by their aerodynamic properties, measuring so-called aerodynamic particle size (d_{ae}) under the assumption of sphericity and unit density.

Since the GRMs have an extremely low density and are more two-dimensional plates than spheres, their aerodynamic size is smaller than the lateral size (projected diameter, d_{proj}) observed in TEM images, as previously discussed.[41] The relation between the aerodynamic and projected diameters can be defined[20] as

$$d_{ae} = \sqrt{\frac{9\pi\rho_{GRM}t_{GRM}d_{proj}}{16\rho_0}}, \quad (4)$$

where t_{GRM} is the GRM platelet thickness, ρ_0 is the unit density, ρ_{GRM} is the GRM bulk density. As the $t_{GRM} \ll d_{proj}$ and

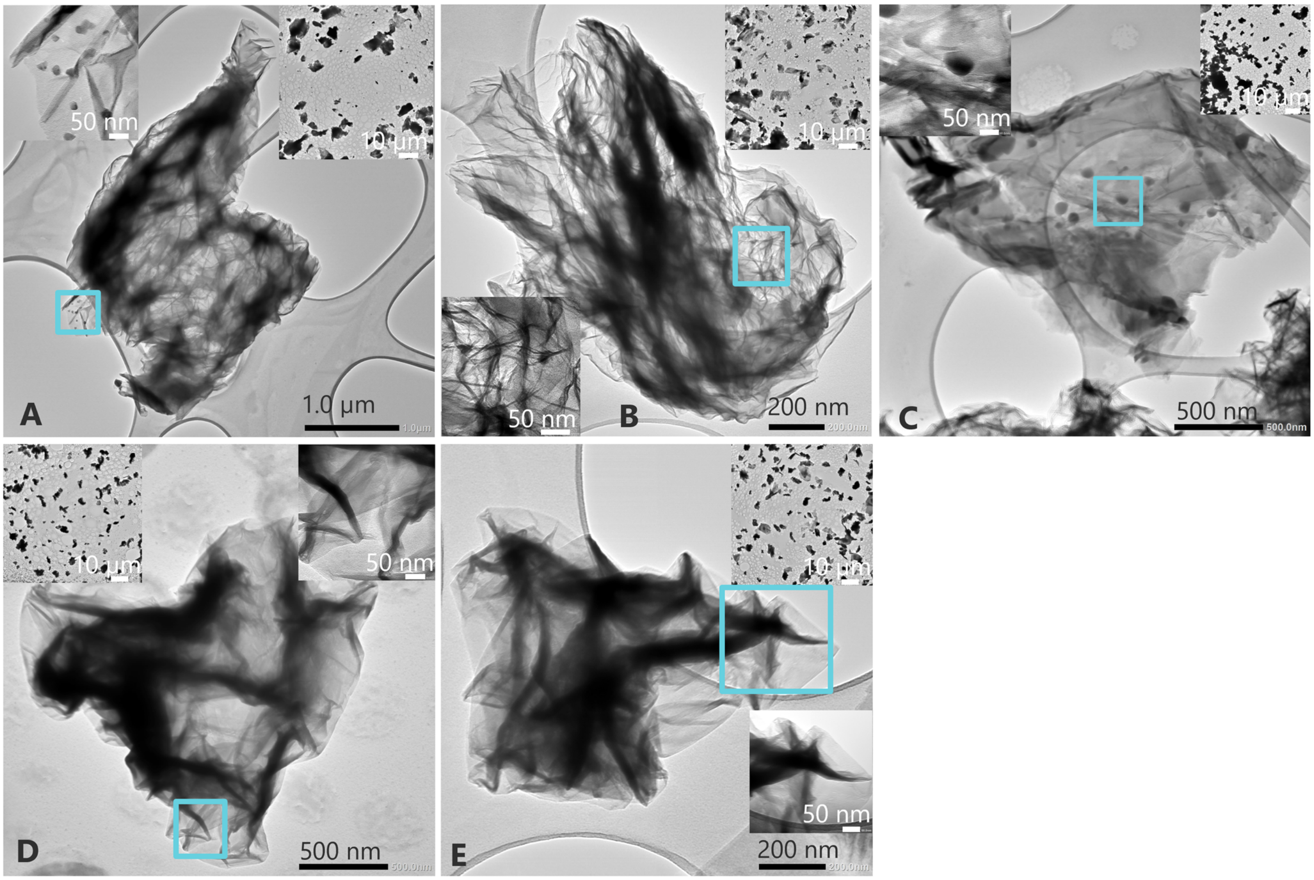

Fig. 3 TEM images of GRM particles collected during dustiness experiments: (A) rGO1, (B) rGO2, (C) rGO3, (D) GO and (E) FLG.

$\rho_{GRM} \ll \rho_0$, the aerodynamic size distribution measured by ELPI is shifted towards smaller particle sizes compared to the lateral size. As GRM behaviour in the human lungs following inhalation is also governed by their aerodynamic properties,[20] the ELPI size distribution is appropriate for lung deposition modelling and subsequent human health risk assessment.

The TEM analyses revealed that the GRM particles are often agglomerated, with small nanoparticles attached to larger micron-sized particles. As shown in Fig. 3, rGO1 and rGO2 exhibit less agglomeration and display a more accordion-shaped structure compared to the other GRMs. This can be attributed to a lower number of oxygen-containing polar groups, which is consistent with the lower moisture content observed for rGO1 and rGO2 relative to rGO3 and GO (Table 1). Consequently, the agglomeration state of the particle population influences the number-based dustiness. As per standard, we tested the materials "as is", without any pretreatment or de-agglomeration procedures. Therefore, the effect of agglomeration on dustiness remains an open question for further studies.

It has also been suggested that effective surface area, which accounts for particle morphology, would serve as a better predictor of the toxicity of carbon-based materials.[80] Therefore, further studies on GRM dustiness should employ alternative approaches, such as surface-based dustiness metrics.[81]

Workplace measurements

Occupational exposure to GRMs was studied in multiple real-world workplace scenarios.

Scenario 1: cell culture treatment with GRM dispersions on a laboratory scale. Release of graphene and personal exposure to GRM were assessed during a cell culture treatment[48,49] with GRM dispersions (0–100 µg mL^{-1}) in a laminar flow cabinet. The PNC at the BZ (1100 ± 700 cm^{-3}) or NF (1300 ± 800 cm^{-3}) was not significantly higher than at the FF (900 ± 700 cm^{-3}) or BG (700 ± 550 cm^{-3}). Therefore, no GRM emissions into workplace air were observed, with no indication of worker exposure.

Scenario 2: GRM powder handling and weighing on a laboratory scale. rGO powder samples (17.5 mL, 12 samples, each rGO1 and rGO2) were prepared and weighed inside a fume hood. As the fume hood's strong airflow affects the weighing result, the airflow was turned off during the task.

rGO emissions were visually observed inside the fume hood, but material transfer to the workplace air was not detected. This was confirmed by the PNC data, which showed a single 3-minute increase (1600 ± 1700 cm^{-3}) inside the fume hood, while PNCs at BZ (420 ± 330 cm^{-3}) and NF (260 ± 300 cm^{-3}) were identical to FF (430 ± 570 cm^{-3}) and BG (280 ± 230 cm^{-3}).

As no GRM transfer to workplace air was detected, worker exposure was deemed minimal, especially given the use of personal protective equipment (PPE), including an FFP3 mask, chemical protective clothing type 5, sleeve covers (Type 5 PB), and two pairs of chemical protective gloves (nitrile rubber).

Scenario 3: GRM powder testing and related maintenance activities in a laboratory. Measures to prevent GRM exposure during handling in a laboratory, *i.e.*, during dustiness testing of rGO1 and rGO2, included technical, personal protective, and organisational solutions. Technical controls included workspace partitioning, combined with a negative-pressure environment, to prevent the possible dispersion of GRM-containing emissions into outside areas. In addition to the use of a fume hood and local exhaust ventilation for the highest exposure potential tasks, personal respiratory protection (a powered filtering device incorporating a hood, TH3P) was utilised, along with chemical protective clothing type 5, sleeve and shoe covers (Type 5 PB), as well as two pairs of disposable chemical protective gloves (nitrile rubber). In addition, waste handling and maintenance were considered, together with communication and warnings to other workers on the premises.

The efficiency of these measures was assessed by detailed aerosol measurements before and during the dustiness testing. The activities included feeding GRM powder samples to the dustiness drum, performing the tests, and cleaning the drum and measurement equipment using dry and wet wiping.

GRM emissions were visually observed in the fume hood, where the drum was filled, emptied, and cleaned, but GRM transport to the workplace air was extremely minor. Outside the fume hood opening, a 15-minute PNC increase (1300 ± 300 cm^{-3}) was observed above BG (250 ± 250 cm^{-3}), and a TEM sample collected simultaneously showed a few graphene-like particles (Fig. S9). Nonetheless, these particles were likely rGO1 dust, similar to those in the dustiness testing samples collected simultaneously (Fig. S10). This confirms that exposure potential exists, though it is minute. A further PNC increase to approximately 3000 cm^{-3} was observed near the rotating drum (15 min TWA of 1700 ± 600 cm^{-3} and a BG of 800 ± 300 cm^{-3}), but the origin of these particles could not be confirmed.

In addition, one incident occurred in which GRM dust was visually released into a partitioned workspace during the dismantling of a measurement device (ELPI) that was clogged with GRM powder. Surprisingly, the PNCs did not increase during this incident. As the release occurred in a sealed chamber with effective exhaust ventilation and negative pressure, the GRM was not transported to other areas. PPE ensured that worker exposure remained minimal.

Scenario 4: synthesis and laser oxidation of graphene in a research laboratory. A laboratory-scale single-layer graphene synthesis[82] using a tube furnace in a clean room and subsequent laser oxidation[83] in a laser laboratory were studied. The amount of graphene handled was extremely small (<0.1 µg), and no significant indication of GRM or other nanoparticle emissions was found in workplace air during the studied tasks.

PNC at the BZ was low, 260 (110) cm^{-3}, and close to the BG level, 80 (70) cm^{-3}, in the laser laboratory (clean room), all below the LOQ of DISCmini (1000 cm^{-3}). EC concentration was also below LOQ in both environments, and the ELPI+ concentration was low (<15 cm^{-3}). TEM samples collected at the source showed individual carbon-based particles (d_p > 1 µm) with a graphene-like two-dimensional fine structure (Fig. S11–S13), but the origin of these particles was difficult to determine due to an extremely low total particle count in the collected samples. As the TEM samples collected from the BZ did not exhibit such particles, the GRM exposure potential was extremely low or negligible during all tasks.

Scenario 5: graphene-containing plastic pellet production at a pilot scale. Occupational exposure measurements were performed at a pilot-scale plastics manufacturing facility, including handling and mixing of dry graphene powder in a fume hood, pouring the graphene powder into a plastic extruder, and producing plastic-graphene pellets (10% graphene, 17% carbon black, 70% COPET, and 3% additives) using a twin-screw compounder (Berstorff ZE25-48D, Berstorff GmbH). High PNCs (5 h TWA) were observed in the NF (57 000 ± 43 000 cm^{-3}; 187 000 ± 163 000 cm^{-3}), FF (274 000 ± 318 000 cm^{-3}) and the BZ (117 000 ± 204 000 cm^{-3}; 138 000 ± 274 000 cm^{-3}), most likely resulting from plastic fumes rather than graphene itself, while BG PNC was approximately 12 000 ± 10 000 cm^{-3}. TEM images and EDX analyses of the air samples showed a few carbon-containing particles with a graphene-like structure (Fig. S14). However, this is not a definitive indication (nor exclusion) of graphene in the collected samples, due to the presence of plastic and carbon black agglomerates (Fig. S15). Nevertheless, worker exposure to graphene was negligible, owing to the use of a fume hood, LEVs, and PPE. However, bystanders without PPE are at considerable risk of exposure to nanoparticles and other carbon-based particles during such processing, underscoring the need for more effective mitigation measures.

Similarly high PNCs (>100 000 cm^{-3}) have been reported previously in carbon fibre processing using FLG-epoxy-solvent baths.[84] The process utilised high-temperature ovens to remove the original coating and dry the newly coated fibres after the bath. The PNC increased immediately after turning on the ovens; thus, the airborne particles might have originated from the high-temperature process, creating polymer and surfactant fumes rather than FLG itself. Nonetheless, FLG exposure could not be excluded, since no data on elemental composition or morphology were reported.

Scenario 6: GO production. During industrial-scale GO manufacturing,[49] the average PNC level (1800 ± 8300 cm^{-3}) during the 7-hour workday (16 November, Table S3) was above background (360 ± 900 cm^{-3}), but remained well below the recommended levels for nanoparticles (40 000 cm^{-3}), as shown in Fig. 4. Similarly, the EC collections from workplace air did not show GO releases near the worker or the process. The typical elements in the TEM samples were most likely process-related precursor materials rather than the actual final GO material. However, individual large (µm-scale) particles with a possible GO sheet structure and high carbon content were detected in all samples (Fig. S16–S28).

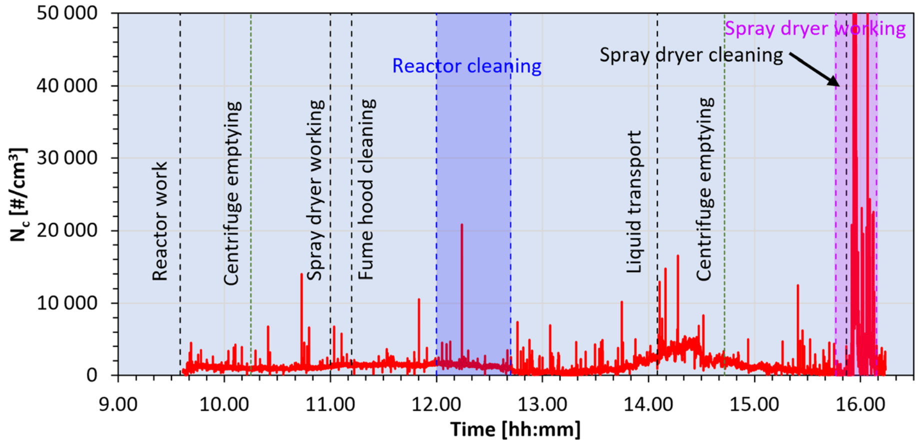

Fig. 4 Particle number concentrations (d_p = 10–700 nm, DISCmini) at the worker's breathing zone during GO production over a 7-hour work shift (Scenario 6).

The results were as expected, since the GO material and precursors were mostly handled in liquid dispersion, which is unlikely to induce airborne emissions in particulate form. As these dispersions were used in closed systems, airborne mists, fumes, or vapours were unlikely to be released, with exposure possible only during leaks. The final synthesis stage, spray drying, was the first stage where dry material was produced and handled.

During this stage, one task, the cleaning of a spray dryer, showed high PNC (16 000 ± 50 000 cm^{-3}, max 460 000 cm^{-3}) and LDSA (55 ± 140 μm^2 cm^{-3}, max 1130 μm^2 cm^{-3}) levels briefly at 15:54–16:08 (Fig. 4). Simultaneous TEM sampling at the BZ indicated particles up to 30 µm in size, though their number was low (Fig. S29), while most detected particles were µm-scale, sheet-like, and had high carbon content (Fig. 5A–C; Fig. S30). EDX analysis indicated that these carbon-rich particles may also contain precursor residues, mainly sulphur, chlorine, and silicon, used in the production. Additionally, particles of approximately 800 nm in length were observed (Fig. 5D), consisting of small primary spheres (*ca.* 20–50 nm; Fig. S31).

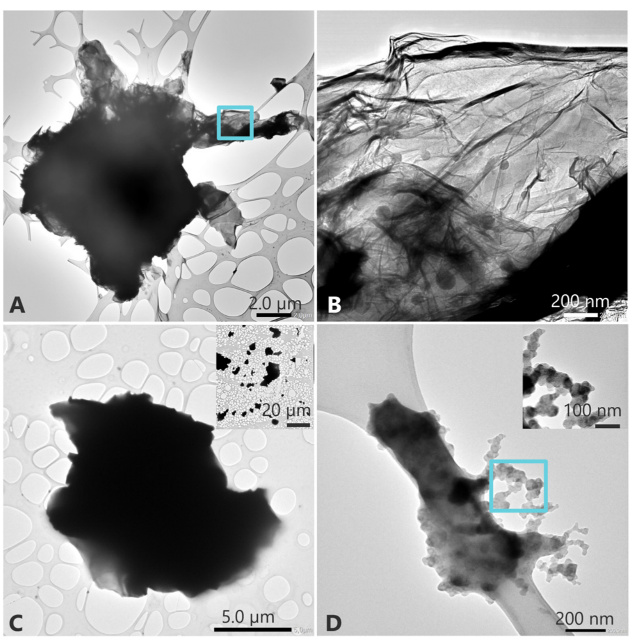

Fig. 5 TEM images of particles collected at the worker's breathing zone during the spray dryer cleaning task in GO production (Scenario 6). (A) GO particle; (B) fine structural detail; (C) large GO particles; and (D) an agglomerate composed of nanoscale primary particles.

For statistical analysis, individual particles (n = 252) from the TEM sample were counted (Fig. 6), indicating a nearly unimodal lognormal size distribution (0.02–0.55 µm), with a geometric mean diameter of 0.08 µm (GSD 1.73) (*a*-axis). The fraction of nanoparticles (≤0.1 µm) was significant: 0.60, 0.73, and 0.31 for the *a*-, *b*-, and *c*-axis, respectively. The average aspect ratio indicated only minor deviation from a spherical shape (Table 2).

The analysis reveals two nanoparticle types: first, approximately 0.1 µm in size and second, smaller 20–50 nm particles. The key difference is that the 0.1 µm particles typically had a halo around them (Fig. S32), indicating remains of condensation over a solid, dense core of the same size (20–50 nm) as the particles detected without the halo. Identification of these 20–50 nm particles is not certain, but they likely originate from the GO manufacturing process, as they consist of C, S, Cl, and Si, similarly to particles >1 µm. DISCmini detected these spheres with a count median diameter (CMD) of 58 nm (GSD 1.83) and a maximum of 300 nm, suggesting the presence of primary particles and their agglomerates.

Analysis of the GO powder (final product) revealed similar particle morphologies and chemical compositions (Fig. S33–S36) as observed in the air samples, confirming the presence of GO- and precursor-originated particles in workplace air.

The particles in the size range 0.55–50 µm (n = 118) also followed a lognormal size distribution with a geometric mean diameter of 4.0 µm (GSD 2.7), as seen in Fig. 6 and Table 2.

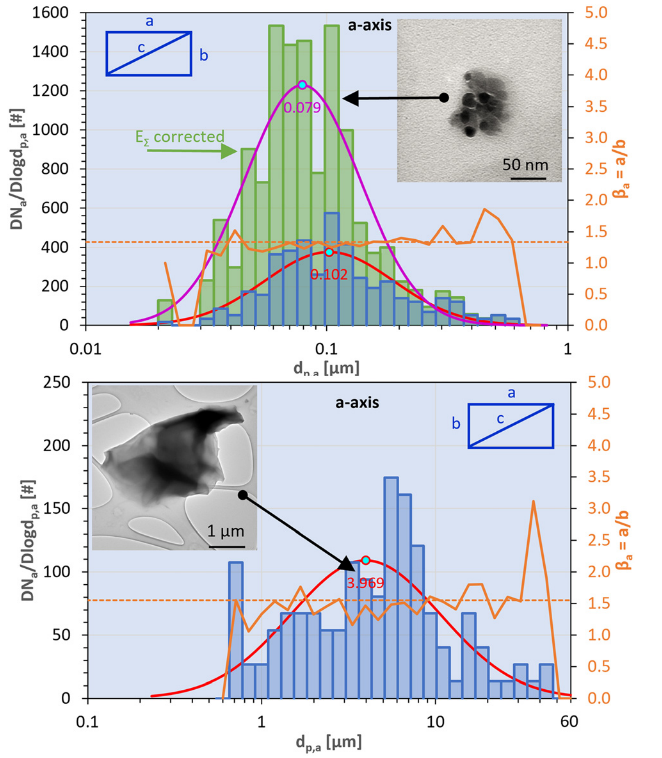

Fig. 6 Number size distribution of 0.02–0.55 μm (n = 252, above) and 0.55–50 μm (n = 118, below) particles for the a-axis. The blue histogram presents the number of counted particles, while the green histogram shows the distribution corrected for collection efficiency (E_Σ).[54,55] Red and pink curves depict fitted lognormal distributions. The orange curve shows the aspect ratio ($\beta = a/b$), with the dotted orange line indicating the average aspect ratio. Examples of particle morphology are displayed as TEM images.

Table 2 Lognormal model-based size distribution parameters (geometric mean diameter, d_p, and geometric standard deviation, σ_g, for a-, b-, and c-axis of the particles) calculated for the 0.02–0.55 μm and 0.55–50 μm size ranges without and (with) collection efficiency (E_Σ) correction[54,55]

	0.02–0.55 μm	0.55–50 μm
N	252	118
$d_{p,a}$ (μm)	0.10 (0.08)	4.0
$d_{p,b}$ (μm)	0.08 (0.07)	2.8
$d_{p,c}$ (μm)	0.13 (0.10)	4.9
$\sigma_{g,a}$	1.85 (1.73)	2.7
$\sigma_{g,b}$	1.82 (1.77)	2.54
$\sigma_{g,c}$	1.83 (1.75)	2.68
$\beta = a/b$	1.30 (1.25)	1.49 (1.44)
σ_β	0.26	0.36
$d_{MMD,a}$ (μm)	0.20	76.4
$d_{MMAD,a}$ (μm)	0.06	34.3
PNC (cm^{-3})	1.6×10^4	1.3×10^3
f_{PNC} (–)	0.925	0.075
M (mg m^{-3})	5×10^{-8}	0.78
f_M (–)	6×10^{-8}	0.99999994

The mean (median) aspect ratio (β) and its standard deviation (σ_β), collection efficiency corrected mass median ($d_{MMD,a}$) and mass median aerodynamic ($d_{MMAD,a}$) diameters, particle number (PNC) and mass (M) concentrations, as well as number (f_{PNC}) and mass (f_M) fractions, are also reported for both size ranges.

The aspect ratio indicates that the particles in this size range were more elongated than those in the smaller size range. This was further verified by the individual particle aspect ratios, which indicated that the fraction of particles with an aspect ratio greater than 1.5 was 0.29, nearly 2.5-fold higher than for the smaller-size range-particles.

Note that the distributions derived from TEM images could differ from aerodynamic or electrical sizing owing to graphene's low density and specific morphology,[85] which may explain differences between, for example, TEM and DISCmini data.

Scenario 7: FLG production. In an FLG production facility,[41] the PNCs remained low during the various stages of the process (Table S4). EC concentration was below LOQ during all tasks, consistent with earlier studies.[32,35]

In one task, during which freeze-dried FLG was handled and treated, the PNC at the BZ averaged 3600 ± 1200 cm^{-3}, not significantly above the BG of 2600 ± 350 cm^{-3}. However, short burst-like increases and decreases in PNC were detected at the BZ and NF, but not in the FF or BG data (Fig. S37). These fluctuations might have resulted from large particles entering the DISCmini device, leading to erroneous particle-detection signals, as previously discussed.[50]

Simultaneous TEM sampling revealed particles with possible FLG-like structures (Fig. S38–S40) measuring 1–3 μm in lateral size. The particles contained C as well as Al, Mg, Si, Ca, and Fe, including trace amounts of S and Cl, indicating residues from precursor materials or process equipment. Moreover, carbon-containing agglomerates (d_p = 0.5–2 μm) consisting of primary spherical particles (d_p < 50 nm) were found, along with aggregates of irregularly shaped 0.5–1 μm particles (Fig. S41 and S42). A large particle (>5 μm) was also detected, rich in Si and Ca (Fig. S43). Thus, FLG emissions to workplace air are possible due to manual scraping of flaky, slate-like FLG from the freeze-dryer plates, as well as from occasional vacuum cleaning.

FLG-like structures rich in Fe and Ca, and similar agglomerates, were also found in TEM samples (Fig. S44–S46) collected during other stages of the process, *i.e.*, handling raw graphite in a fume hood and liquid-phase exfoliation of graphite,[86] but the PNC remained near BG levels during these tasks. Similar observations of particle morphology and composition were made from TEM samples collected during manual loading of a freeze-dryer and handling of the freeze-dryer plates (Fig. S47–S51). These tasks also showed slight PNC increases at the BZ and NF above the BG level (Fig. S52).

Apart from these releases during handling of freeze-dried FLG and the dryer plates, FLG-containing particle or other aerosol emissions were minimal in the manufacturing process, due to the use of closed systems and fume hoods, or because the FLG materials, precursors, and intermediates were in a liquid state. As a result of low airborne GRM concentrations and regular use of PPE, worker exposure potential remains low.

An earlier study[41] in the same work environment observed similar PNC levels (3100–5100 cm^{-3}) during FLG production, but due to a high BG (4500–5600 cm^{-3}), process-related releases were not apparent. However, the presence of FLG in the aerosol samples was confirmed *via* TEM imaging as well as EDX and Raman spectroscopies, showing particles consisting of carbon atoms with few bonded oxygen atoms.

Exposure modelling

Exposure to GRMs was modelled in three simulated scenarios, assuming GRM emission rates derived from the dustiness testing, according to eqn (1). The PNCs at the BZ were modelled assuming only general ventilation as a mitigation measure.

Scenario 8: laboratory-scale powder handling. In this scenario, a small amount (17.5 mL min^{-1}, 0.08–3.5 g min^{-1}, total 2.4–105 g) of GRM was handled in a small room (4 × 4 × 2.5 m^3) with a low air ventilation rate (0.5 h^{-1}) typical of an office, as in Scenarios 1–3. Fig. 7a shows the resulting PNCs for five GRMs at various distances from the source. The PNCs remain below the NRVs for all materials except rGO3. In comparison, similar powder handling in a larger laboratory environment (9 × 6 × 3 m^3) with a higher air ventilation rate (18 h^{-1}) results in much lower PNCs (Fig. 7b). Thus, the utilisation of efficient general ventilation leads to lower exposures. However, very close to the source at 0.2 m, the PNC remains above the NRV_{8h} for rGO3.

Scenario 9: pilot-scale handling or manufacturing. The same GRMs are assumed to be handled at pilot scale (10-fold, 175 mL min^{-1}, 0.8–35 g min^{-1}, total 24–1050 g) in a similar laboratory environment with high air ventilation. This results in near-source PNCs (0.2 m) above both NRVs for rGO3 and FLG (Fig. 7c), indicating a greater overall exposure potential.

Scenario 10: industrial-scale handling or manufacturing. GRM manufacturing at aindustrial-scale (100-fold, 1750 mL min^{-1}, 8–350 g min^{-1}, total 240–10 500 g) in a factory Hall (30 × 20 × 7 m^3) results in considerable near-source PNCs for all materials, 2.5–75 times the NRV_{15min}. However, the PNCs decrease rapidly at greater distances due to efficient air ventilation (18 h^{-1}).

We consider the PNCs at 0.2 metres from the source (2 × 10^5 to 6 × 10^6 cm^{-3}) as a reasonable worst-case estimate of GRM exposure during production upscaling. The PNCs were converted to mass concentrations using eqn (3). The resulting 15 min TWA exposure concentrations range from 7 μg m^{-3} to 6 mg m^{-3}, which are used in the lung deposition calculations.

Lung deposition modelling

The deposition of GRMs in human and rat lungs was modelled for the scenarios with the highest exposure potential, namely Scenarios 6 (real-world) and 10 (reasonable worst-case). Table S5 presents the particle size distributions and aerosol concentrations used as input data for the lung deposition modelling, while Fig. 8a and Table S6 show the results.

Lung deposition modelling (simulations no. 1 and 2) was performed for the spray dryer cleaning task in Scenario 6, based on two different estimates of airborne GO. The first

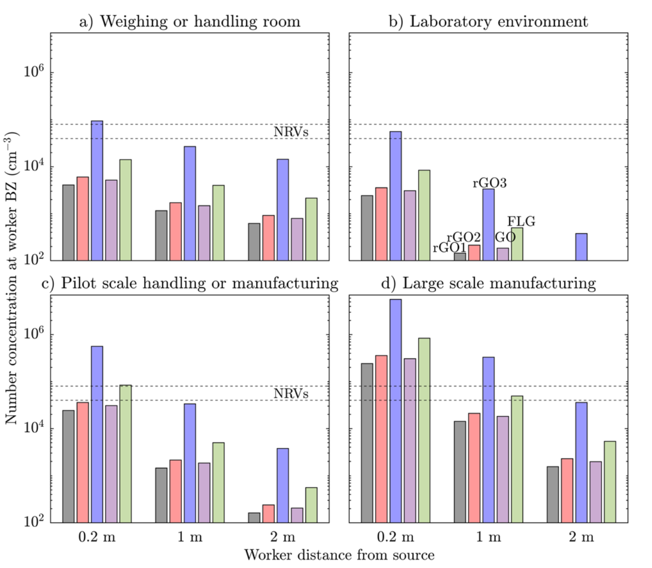

Fig. 7 Modelled number concentrations at the worker's breathing zone, shown as bars from left to right, for rGO1 (black), rGO2 (red), rGO3 (blue), GO (purple) and FLG (green). Laboratory-scale powder handling in (a) weighing room (4 × 4 × 2.5 m^3, 0.5 h^{-1}) and (b) laboratory environment (9 × 6 × 3 m^3, 18 h^{-1}); (c) pilot-scale (10-fold) handling or manufacturing in a similar laboratory environment; and (d) industrial-scale (100-fold) manufacturing in a factory Hall (30 × 20 × 7 m^3, 18 h^{-1}). The nano reference values (NRVs) for 8 h and 15 min exposures (40 000 and 80 000 cm^{-3}) are indicated with horizontal dashed lines. Note the logarithmic *y*-axis.

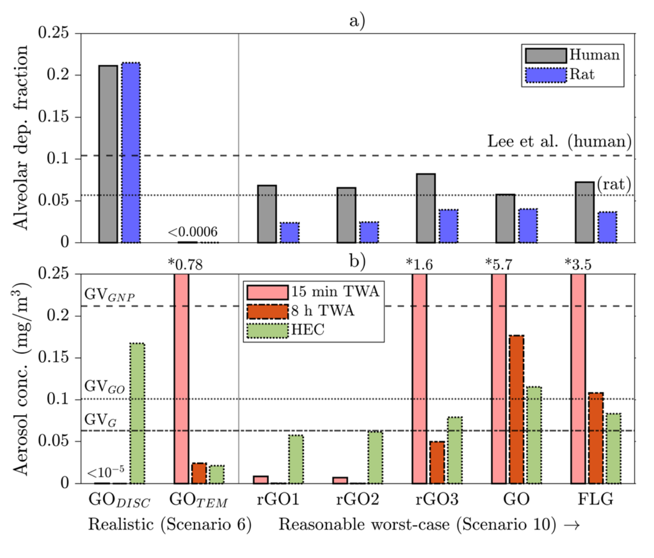

Fig. 8 (a) Modelled alveolar deposition fractions in human and rat respiratory tracts for seven MPPD simulations covering multiple GRMs. Horizontal lines represent comparable values calculated for GO by Lee *et al.*[65] (b) Exposure concentrations (red) as 15 min and 8 h time weighted averages (TWA) for a real-world exposure (Scenario 6) based on workplace sampling with DISCmini (GO_{DISC}) and electron microscopy (GO_{TEM}). Reasonable worst-case exposure estimates (Scenario 10) are based on exposure modelling. Calculated human equivalent concentrations (HEC, green) are based on the no-observed adverse-effect concentration in rats.[66] Horizontal lines indicate guidance values for graphene nanoplatelets (GV_{GNP},[74] GV_G[75]) and GO (GV_{GO})[75] extracted from the literature.

simulation (#1) was based on DISCmini (10–700 nm) PNC measurement data at the BZ, leading to predominantly alveolar deposition (21%) with a relatively low alveolar mass deposition rate (1.33×10^{-3} μg min^{-1}) due to small particle size (CMD 58 nm). For an exposure time of 30 min day^{-1} for 90 days, the alveolar mass retained in human (rat) lungs is 3.6 (0.06) μg.

The second simulation (#2) of the same task was based on a bimodal particle size distribution calculated from the TEM analysis (Fig. 6 and Table 2), providing a more realistic estimate of the GO particle population. In this case, particles were deposited mainly in the head airways (61%), while alveolar deposition accounted for only 0.06%. However, the alveolar deposition rate of 8.87×10^{-3} μg min^{-1} was sevenfold higher due to large (MMAD 34 μm, CMD 4 μm) particles dominating the mass size distribution. For an exposure time of 30 min day^{-1} for 90 days, the alveolar mass retained in human (rat) lungs is 24 (0.05) μg.

Furthermore, lung deposition was estimated for exposure Scenario 10 (simulations no. 3–7). The mass deposition to the alveolar region (6–8%) leads to an alveolar retained GRM mass of 0.02–17 mg in human lungs, and 0.15 μg to 0.20 mg in rat lungs, after a 90-day exposure period. Similarly, Lee *et al.*[65] calculated alveolar masses retained of approximately 30 mg in human and *ca.* 1 mg in rat lungs. Such doses have shown adverse effects in experimental animals after pulmonary exposure,[24] but they depend on the application method, species, and GRM properties.[8]

Su *et al.*[26] measured graphene (platelets, electrical mobility diameter d_B = 51, 101, and 215 nm) deposition, observing 10% cumulative deposition to the head and upper tracheobronchial airways, concluding that the majority of the particles can transit to the alveolar region. In contrast, the GRMs in this study show much higher deposition fractions to the upper airways, approximately 20–90%, while a smaller portion penetrates and eventually deposits in the alveolar region. The difference between the studies may result from the de-agglomeration performed by Su *et al.*, since the graphene powder was broken into small nanoscale primary particles that can penetrate deeper into the lungs. In real workplace environments, the GRM particle size range can vary widely, including primary nanoparticles, their agglomerates, and larger micron-sized particles, as seen, for example, in Scenario 6 of this study. Therefore, it is justified to perform experiments and simulations on raw, untreated materials rather than pre-treated, deagglomerated samples.

Lee *et al.* found an alveolar deposition fraction of 10% for GO powder (MMAD 0.2 μm), whereas in this study, the modelled deposition of GO powder (MMAD 0.8 μm) was 6%. On the other hand, in GO manufacturing (Scenario 6 of this study), the alveolar deposition was 21% for 0.06 μm (MMAD) and 0.06% for 34 μm particles. The differences in alveolar deposition are therefore likely due to the different particle sizes employed in the studies. Since the MPPD model considers only mass-based distributions, nanoparticles are marginalised in the calculation of alveolar deposition fractions. Thus, a number- or surface area-based deposition calculation may provide better insight into nanoscale GRM deposition.

Inhalation toxicity and health risk assessment

The health effects on the lungs are frequently studied using inhalation experiments. Inhalation toxicity studies conducted to date for GRMs are summarised in Table S7. In all studies, lung inflammation was considered a relevant endpoint, as it is commonly used for setting OELs.

Short inhalation exposures (maximum 5 days) to GRMs have shown inflammatory effects in rat lungs,[66,68,70,71] specifically increased neutrophils in bronchoalveolar lavage (BAL) fluid. The NOAECs ranged from 0.5 to 9.8 mg m^{-3} across studies.

A 28-day inhalation study of GNPs (MMAD 0.123 μm, GSD 3.63)[69] showed no adverse effects in rats, even at the highest concentration of 1.88 mg m^{-3}. Based on this sub-acute study, Spinazzè *et al.*[74] calculated a health-based guidance value (GV_{GNP}) of 0.212 ± 7.796 mg m^{-3} using a probabilistic method, and Pitaro *et al.*[75] derived a DNEL (here GV_G) of 0.063 μg m^{-3} based on ECHA guidance (Chapter R.8), applying an uncertainty factor (UF) of 30 to the NOAEC.

A 90-day subchronic study[65] exposed rats to GO aerosol (MMAD 0.20 μm, GSD 2.01), with NOAEC at the highest dose of 3.02 mg m^{-3}. They calculated an HEC of 0.54 mg m^{-3} and proposed a GV of 0.018 mg m^{-3} (UF 30). However, the experimental data were not fully presented, making it difficult to evaluate the results. Later, Pitaro *et al.*[75] calculated a DNEL (here GV_{GO}) of 0.101 μg m^{-3} based on the NOAEC.

As neither of these inhalation studies reported any toxic effects, inference is limited. According to OECD guidelines 412 [87] and 413,[88] the highest dose should induce toxic effects to reliably estimate NOAECs. This was addressed in a 28-day inhalation study[67] on single-layer graphene, which showed an increased neutrophil count in BAL as well as increased lactate dehydrogenase, both markers of lung inflammation. A NOEAC of 0.8 mg m^{-3} was derived. However, in a subsequent study, no toxic effects were found for GNPs at the highest dose of 3.2 mg m^{-3}.

Furthermore, Andrews *et al.*[89] exposed healthy human volunteers to GO nanosheets (CMD 0.15 and 0.43 μm) at *circa* 0.2 mg m^{-3}. No acute adverse respiratory or cardiovascular effects were observed after 2-hour exposure, although larger super-micron GO sheets were excluded for safety, as they had shown adverse effects in experimental animals.

Studies have generally shown lower NOAEC values for graphene than for GO; however, these results are not fully comparable due to variations in dosing and GRM properties (lateral size, thickness, surface area, and agglomeration; Table S7). Thus, limited data on the inhalation toxicity of GRMs complicates health risk assessment. Currently, all guidance values are based on two inhalation studies[65,69] that did not show adverse effects at the highest dose, so the GV calculation requires revision.

As a conservative approach, the lowest available NOAEC of 0.5 mg m^{-3} in rats, five times lower than the lowest-observed-adverse-effect level, was used to calculate HECs. With modelled rat-to-human translation factors (NOAEC/HEC) of 3–23, HECs for the GRMs in this study range from 0.02 to 0.17 mg m^{-3} (presented in Fig. 8b). These values are similar to the GVs (0.018–0.212 mg m^{-3}) derived from higher NOAECs in previous studies.[65,74,75]

Fig. 8b also presents exposure concentrations for measured real-world (Scenario 6) and modelled worst-case (Scenario 10) situations. The 8-hour (TWA) exposure concentrations are below the "upper limit of health-based guidance values" or GV_{GNP} of 0.212 mg m^{-3}. However, for GO and FLG, the 8-hour exposures exceed both GV_{GO} and GV_{G}, and are also above their respective HECs for GO_{TEM}, GO, and FLG, resulting in risk characterisation ratios above unity: 1.1, 1.5, and 1.3, respectively. A common factor is that these materials mostly consist (by mass) of super-micron particles. By contrast, GO_{DISC} and rGO 1–3, consisting of nanoscale and submicron particles, had much lower RCRs (0.00006 to 0.6).

The real-world scenario (current use) produced mixed results. While 8-hour exposures were below literature GVs for both nanoscale (GO_{DISC}) and super-micron (GO_{TEM}) GO particles, the RCR for GO_{TEM} is slightly above unity due to a low HEC. Thus, given limited information on chronic effects at low exposures, adverse effects cannot be excluded if appropriate worker protection is not in place. This is especially relevant, as preliminary control banding suggests that even concentrations below 10 μg m^{-3} may have adverse effects.[90]

The realistic worst-case scenario (potential future use with increased GRM production) results in high exposures for GO and FLG, increasing health risks and highlighting the need for effective mitigation measures. As future uses may increase health risks, our results emphasise the need to reassess whenever activities, processes, or materials change.

As the health risk assessment is currently limited to acute and sub-acute studies, further inhalation toxicity investigations on the chronic effects of GRMs are needed, with accurate and appropriate dosing to enable reliable OEL determination. In addition to a full work shift (8 h) exposure, an OEL should also be set for short-term (15 min) exposures, since GRM-releasing tasks can be brief but produce high concentration peaks.

A further limitation in the health risk assessment arises from uncertainty in the estimated exposure concentration and HEC values. Uncertainty propagates as multiple assessment steps are concatenated. Since uncertainty has only been quantified for certain steps of this study, the assessment presented here should be considered an estimate. Future efforts should aim to reduce uncertainties throughout the assessment process.

Conclusions

Occupational safety aspects of graphene-related material production and handling were evaluated through exposure and risk assessments conducted in five workplaces. These assessments were complemented by characterisation and dustiness testing of selected GRMs, which were utilised for exposure and lung deposition modelling.

Exposure and risk in GRM production and related activities were generally low, owing to appropriate occupational hygiene measures at organisational, technical, and personal levels. Activities that posed an increased health risk included handling GRMs in dry powder form and the cleaning of process equipment contaminated with dry GRM. While traditional occupational and nanosafety practices[91] are suitable and recommended, continuous vigilance to mitigate potential risks is necessary, particularly when planning changes or developing activities, processes, or materials.[42,84,92–94]

Scale-up, changes in material quantities or raw materials, new processing techniques or equipment, and organisational aspects such as personnel changes all contribute to potential GRM exposure. Given the limited information on chronic health effects, the precautionary principle is advised in workplace safety considerations. A "best practices for safe graphene work" guidance document is available online in four languages (English, Finnish, Italian, and Spanish),[95] providing information on specific GRM safety aspects alongside general nano- and occupational safety guidelines.

To further advance knowledge and understanding of GRM exposure and risk in occupational environments, state-of-the-art measurement and analysis technologies should be adopted,[96] as instrumentation continues to evolve. At the same time, regulatory frameworks are progressing and establishing safety standards in this field.[97–99] Keeping pace with these developments may benefit from adopting the Safe and Sustainable by Design (SSbD) approach.[75,100]

Author contributions

Conceptualization: M. P., T. K.; data curation: M. P., T. K., J. L., A. I.; formal analysis: M. P., J. L., A. I., T. K.; funding acquisition: T. K.; investigation: M. P., T. K., M. L., A. I., K. A.; methodology: M. P., T. K., J. L., P. H.; project administration: T. K.; resources: T. K., M. P., K. A., J. G.; software: M. P., A. I., P. H.; supervision: T. K., M. P.; validation: M. P., J. L., K. A.; visualization: M. P., J. L., A. I., T. K.; writing-original draft: M. P.; writing-review & editing: M. P., J. L., A. I., K. A., P. H., M. L., J. W.-L., J. G., T. K.

Conflicts of interest

There are no conflicts to declare.

Data availability

The data supporting this article are included as part of the supplementary information (SI): TEM images, EDX spectra, particle number concentration figures, measurement notes, modelling input and output values (SI.pdf); additional TEM images, EDX spectra (additional TEM and EDX data.pdf). See DOI: https://doi.org/10.1039/d5nr01885d.

Further data for this article, including measurement and modelling data files, and data analysis scripts, are available at Zenodo at https://doi.org/10.5281/zenodo.15385012. The source code for the exposure model is available at https://gitlab.com/MiPo/indoorturbulentdiffusion. The code version used in this study corresponds to commit a62d5e071826ec7907aeb9ba75aab10a94c06a84.

Acknowledgements

This study was funded by the European Commission as part of the Graphene Flagship Core 3 research initiative (Grant Agreement ID: 881603). M. P. acknowledges financial support from the Finnish Work Environment Fund (Grant ID: 240406).

We gratefully acknowledge the personnel at the Finnish Institute of Occupational Health: Sampsa Törmänen for assistance with workplace measurements; Pasi Polvi for technical support in assembling the dustiness testing setup; Marja Laitia, Päivi Tuominen, Huong Ly, and Anneli Hännikäinen for the EC analyses; and Julia Catalán for collaboration in funding acquisition, establishing contacts with GRM companies, and facilitating laboratory access for exposure measurements.

We also thank Jani Pelto at VTT Technical Research Centre of Finland and Mika Pettersson at the Nanoscience Center, University of Jyväskylä, Finland, for providing access to GRM workplaces for exposure measurements. We are grateful to Beatriz Alonso at Graphenea, Spain, and Antonio Esau Del Rio Castillo at BeDimensional, Italy, for providing workplace access and for supplying GRMs for dustiness testing. We thank all workers who participated in the exposure measurements.

Special thanks to Bengt Fadeel at Karolinska Institutet, Sweden, for valuable discussions throughout this study.

During the finalisation of this manuscript, the Perplexity AI Online tool was utilised between 3 and 16 May 2025. The following advanced language models were accessed *via* Perplexity Online: Perplexity AI (version 3.2.0, released 26 November 2024), OpenAI GPT-4o (released 13 May 2024), Anthropic Claude 3.5 Sonnet (released 20 June 2024), and Google Gemini 2.5 Pro (released 25 March 2025). In addition, Grammarly (version 1.2.158.1663, downloaded 7 May 2025) was used on 7–8 May 2025 and 29 October 2025. These tools were employed to provide suggestions for English language correction and refinement. An initial version of this disclosure statement on AI usage was generated by Perplexity Online. All outputs generated by these tools were critically reviewed, edited, and individually implemented by the corresponding author (M. P.). The authors take full responsibility for the content and scientific integrity of the work.

References

1 A. C. Ferrari, F. Bonaccorso, V. Fal'ko, K. S. Novoselov, S. Roche, P. Bøggild, S. Borini, F. H. L. Koppens, V. Palermo, N. Pugno, J. A. Garrido, R. Sordan, A. Bianco, L. Ballerini, M. Prato, E. Lidorikis, J. Kivioja, C. Marinelli, T. Ryhänen, A. Morpurgo, J. N. Coleman, V. Nicolosi, L. Colombo, A. Fert, M. Garcia-Hernandez, A. Bachtold, G. F. Schneider, F. Guinea, C. Dekker, M. Barbone, Z. Sun, C. Galiotis, A. N. Grigorenko, G. Konstantatos, A. Kis, M. Katsnelson, L. Vandersypen, A. Loiseau, V. Morandi, D. Neumaier, E. Treossi, V. Pellegrini, M. Polini, A. Tredicucci, G. M. Williams, B. H. Hong, J.-H. Ahn, J. M. Kim, H. Zirath, B. J. Van Wees, H. Van Der Zant, L. Occhipinti, A. Di Matteo, I. A. Kinloch, T. Seyller, E. Quesnel, X. Feng, K. Teo, N. Rupesinghe, P. Hakonen, S. R. T. Neil, Q. Tannock, T. Löfwander and J. Kinaret, *Nanoscale*, 2015, **7**, 4598–4810.

2 J. Domenech, A. Rodríguez-Garraus, A. López De Cerain, A. Azqueta and J. Catalán, *Nanomaterials*, 2022, **12**, 1795.

3 B. Fadeel, C. Bussy, S. Merino, E. Vázquez, E. Flahaut, F. Mouchet, L. Evariste, L. Gauthier, A. J. Koivisto, U. Vogel, C. Martín, L. G. Delogu, T. Buerki-Thurnherr, P. Wick, D. Beloin-Saint-Pierre, R. Hischier, M. Pelin, F. C. Carniel, M. Tretiach, F. Cesca, F. Benfenati, D. Scaini, L. Ballerini, K. Kostarelos, M. Prato and A. Bianco, *ACS Nano*, 2018, **12**, 10582–10620.

4 Ó. Cebadero-Domínguez, A. Jos, A. M. Cameán and G. M. Cătunescu, *Food Chem. Toxicol.*, 2022, **164**, 113014.

5 A. Bianco, A. Del Rio, G. Varchi, M. D. Parenti and V. Palermo, *Assessment of the potential impact of graphene, graphene oxide and other 2D materials on health, and the environment: June 2022*, ECHA, Helsinki, 2022.

6 X. Ding, Y. Pu, M. Tang and T. Zhang, *Nano Today*, 2022, **42**, 101379.

7 P. Govindaraj, A. Mirabedini, X. Jin, D. Antiohos, N. Salim, P. Aitchison, J. Parker, F. K. Fuss and N. Hameed, *J. Mater. Sci. Technol.*, 2023, **155**, 10–32.

8 C. Kong, J. Chen, P. Li, Y. Wu, G. Zhang, B. Sang, R. Li, Y. Shi, X. Cui and T. Zhou, *Toxics*, 2024, **12**, 82.

9 H. Lin, T. Buerki-Thurnherr, J. Kaur, P. Wick, M. Pelin, A. Tubaro, F. C. Carniel, M. Tretiach, E. Flahaut, D. Iglesias, E. Vázquez, G. Cellot, L. Ballerini, V. Castagnola, F. Benfenati, A. Armirotti, A. Sallustrau, F. Taran, M. Keck, C. Bussy, S. Vranic, K. Kostarelos, M. Connolly, J. M. Navas, F. Mouchet, L. Gauthier, J. Baker, B. Suarez-Merino, T. Kanerva, M. Prato, B. Fadeel and A. Bianco, *ACS Nano*, 2024, **18**, 6038–6094.

10 H. Jin, N. Lai, C. Jiang, M. Wang, W. Yao, Y. Han and W. Song, *Processes*, 2025, **13**, 209.

11 B. Fadeel, J. Baker, L. Ballerini, C. Bussy, F. C. Carniel, M. Tretiach, M. Pelin, T. Buerki-Thurnherr, T. Kanerva, J. M. Navas, E. Vázquez, V. Rodriguez Unamuno, P. Lehtonen, M. González, H. Rauscher, J. Riego Sintes, K. Kostarelos, A. Bianco and M. Prato, *Small*, 2025, **21**, 2404570.

12 M. C. Duch, G. R. S. Budinger, Y. T. Liang, S. Soberanes, D. Urich, S. E. Chiarella, L. A. Campochiaro, A. Gonzalez, N. S. Chandel, M. C. Hersam and G. M. Mutlu, *Nano Lett.*, 2011, **11**, 5201–5207.
13 S. Bengtson, K. B. Knudsen, Z. O. Kyjovska, T. Berthing, V. Skaug, M. Levin, I. K. Koponen, A. Shivayogimath, T. J. Booth, B. Alonso, A. Pesquera, A. Zurutuza, B. L. Thomsen, J. T. Troelsen, N. R. Jacobsen and U. Vogel, *PLoS One*, 2017, **12**, e0178355.
14 T. Loret, L. A. V. De Luna, A. Fordham, A. Arshad, K. Barr, N. Lozano, K. Kostarelos and C. Bussy, *Adv. Sci.*, 2022, **9**, 2104559.
15 B. Li, J. Yang, Q. Huang, Y. Zhang, C. Peng, Y. Zhang, Y. He, J. Shi, W. Li, J. Hu and C. Fan, *NPG Asia Mater.*, 2013, **5**, e44.
16 X. Wang, M. C. Duch, N. Mansukhani, Z. Ji, Y.-P. Liao, M. Wang, H. Zhang, B. Sun, C. H. Chang, R. Li, S. Lin, H. Meng, T. Xia, M. C. Hersam and A. E. Nel, *ACS Nano*, 2015, **9**, 3032–3043.
17 A. F. Rodrigues, L. Newman, D. Jasim, S. P. Mukherjee, J. Wang, I. A. Vacchi, C. Ménard-Moyon, A. Bianco, B. Fadeel, K. Kostarelos and C. Bussy, *Adv. Sci.*, 2020, **7**, 1903200.
18 T. Loret, L. A. V. De Luna, M. A. Lucherelli, A. Fordham, N. Lozano, A. Bianco, K. Kostarelos and C. Bussy, *Small*, 2023, **19**, 2301201.
19 L. A. V. De Luna, T. Loret, A. Fordham, A. Arshad, M. Drummond, A. Dodd, N. Lozano, K. Kostarelos and C. Bussy, *Part. Fibre Toxicol.*, 2022, **19**, 62.
20 A. Schinwald, F. A. Murphy, A. Jones, W. MacNee and K. Donaldson, *ACS Nano*, 2012, **6**, 736–746.
21 K. Wu, Q. Zhou and S. Ouyang, *Nanomaterials*, 2021, **11**, 2889.
22 H. N. du Preez and M. Halma, *Nano Biomed. Eng.*, 2024, **16**, 219–231.
23 S. S. Poulsen, S. Bengtson, A. Williams, N. R. Jacobsen, J. T. Troelsen, S. Halappanavar and U. Vogel, *Toxicol. Appl. Pharmacol.*, 2021, **410**, 115343.
24 S. Chortarea, O. C. Kuru, W. Netkueakul, M. Pelin, S. Keshavan, Z. Song, B. Ma, J. Gómes, E. V. Abalos, L. A. V. D. Luna, T. Loret, A. Fordham, M. Drummond, N. Kontis, G. Anagnostopoulos, G. Paterakis, P. Cataldi, A. Tubaro, C. Galiotis, I. Kinloch, B. Fadeel, C. Bussy, K. Kostarelos, T. Buerki-Thurnherr, M. Prato, A. Bianco and P. Wick, *J. Hazard. Mater.*, 2022, **435**, 129053.
25 M. Pelin, S. Sosa, M. Prato and A. Tubaro, *Nanoscale*, 2018, **10**, 15894–15903.
26 W.-C. Su, B. K. Ku, P. Kulkarni and Y. S. Cheng, *J. Occup. Environ. Hyg.*, 2016, **13**, 48–59.
27 W. A. Heitbrink, L.-M. Lo and K. H. Dunn, *J. Occup. Environ. Hyg.*, 2015, **12**, 16–28.
28 A. Spinazzè, A. Cattaneo, D. Campagnolo, V. Bollati, P. A. Bertazzi and D. M. Cavallo, *Aerosol Sci. Technol.*, 2016, **50**, 812–821.
29 A. Spinazzè, A. Cattaneo, F. Borghi, L. Del Buono, D. Campagnolo, S. Rovelli and D. M. Cavallo, *Med. Lav.*, 2018, **109**, 285–296.
30 F. Boccuni, R. Ferrante, F. Tombolini, D. Lega, A. Antonini, A. Alvino, P. Pingue, F. Beltram, L. Sorba, V. Piazza, M. Gemmi, A. Porcari and S. Iavicoli, *Int. J. Mol. Sci.*, 2018, **19**, 349.
31 I. Iavicoli, L. Fontana, P. Pingue, A. M. Todea and C. Asbach, *Sci. Total Environ.*, 2018, **627**, 689–702.
32 J. H. Lee, J. H. Han, J. H. Kim, B. Kim, D. Bello, J. K. Kim, G. H. Lee, E. K. Sohn, K. Lee, K. Ahn, E. M. Faustman and I. J. Yu, *Inhalation Toxicol.*, 2016, **28**, 281–291.
33 I. Bellagamba, F. Boccuni, R. Ferrante, F. Tombolini, F. Marra, M. S. Sarto and S. Iavicoli, *Nanomaterials*, 2020, **10**, 1520.
34 I. Bellagamba, F. Boccuni, R. Ferrante, F. Tombolini, C. Natale, F. Marra, M. S. Sarto and S. Iavicoli, *Nanomaterials*, 2023, **13**, 1378.
35 C. Vaquero, R. Wendelbo, A. Egizabal, C. Gutierrez-Cañas and J. López de Ipiña, *J. Phys.: Conf. Ser.*, 2019, **1323**, 012005.
36 K. Lovén, S. M. Franzén, C. Isaxon, M. E. Messing, J. Martinsson, A. Gudmundsson, J. Pagels, M. Hedmer, N. Lund, K. Lovén, S. M. Franzén, C. Isaxon, M. E. Messing, A. Gudmundsson, J. Pagels and M. Hedmer, *J. Exposure Sci. Environ. Epidemiol.*, 2021, **31**, 736–752.
37 T. Storsjö, H. Tinnerberg, J. Sun, C. Ruiqi and A. Farbrot, *NanoImpact*, 2024, **33**, 100499.
38 C. Fito López, I. Colmenar González, O. Andreu Sánchez, V. Vela and M. Domat Rodriguez, *Sustainability*, 2023, **15**, 12544.
39 W. Netkueakul, D. Korejwo, T. Hammer, S. Chortarea, P. Rupper, O. Braun, M. Calame, B. Rothen-Rutishauser, T. Buerki-Thurnherr, P. Wick and J. Wang, *Nanoscale*, 2020, **12**, 10703–10722.
40 F. Boccuni, R. Ferrante, F. Tombolini, C. Natale, A. Gordiani, S. Sabella and S. Iavicoli, *Nanotoxicology*, 2020, **14**, 1280–1300.
41 F. Tombolini, F. Boccuni, R. Ferrante, C. Natale, L. Marasco, E. Mantero, A. E. Del Rio Castillo, L. Leoncino, V. Pellegrini, S. Sabella and S. Iavicoli, *Nanoscale*, 2021, **13**, 3841–3852.
42 C. Natale, F. Tombolini, R. Ferrante, F. Sebastiani, A. Gordiani, M. Manigrasso, A. E. Del Rio Castillo, F. Bonaccorso, S. Sabella and F. Boccuni, *NanoImpact*, 2025, **38**, 100555.
43 M. A. E. Plinke, R. Maus and D. Leith, *Am. Ind. Hyg. Assoc. J.*, 1992, **53**, 325–330.
44 K. H. Dunn, A. C. Eastlake, M. Story and E. D. Kuempel, *Ann. Work Exposures Health*, 2018, **62**, 362–388.
45 C. Ribalta, A. C. Ø. Jensen, N. Shandilya, C. Delpivo, K. A. Jensen and A. S. Fonseca, *NanoImpact*, 2024, **33**, 100493.
46 A. S. Fonseca, C. Ribalta, N. Shandilya, W. Fransman and K. A. Jensen, *Ann. Work Exposures Health*, 2024, **68**, 295–311.
47 C. Dazon, O. Witschger, S. Bau, R. Payet, K. Beugnon, G. Petit, T. Garin and L. Martinon, *J. Phys.: Conf. Ser.*, 2017, **838**, 012005.

48 A. Rodríguez-Garraus, C. Passerino, G. Vales, M. Carlin, S. Suhonen, A. Tubaro, J. Gómez, M. Pelin and J. Catalán, *Nanotoxicology*, 2023, **17**, 471–495.
49 M. Pelin, C. Passerino, A. Rodríguez-Garraus, M. Carlin, S. Sosa, S. Suhonen, G. Vales, B. Alonso, A. Zurutuza, J. Catalán and A. Tubaro, *Nanomaterials*, 2023, **13**, 2189.
50 M. Fierz, C. Houle, P. Steigmeier and H. Burtscher, *Aerosol Sci. Technol.*, 2011, **45**, 1–10.
51 J. Keskinen, K. Pietarinen and M. Lehtimäki, *J. Aerosol Sci.*, 1992, **23**, 353–360.
52 A. Järvinen, M. Aitomaa, A. Rostedt, J. Keskinen and J. Yli-Ojanperä, *J. Aerosol Sci.*, 2014, **69**, 150–159.
53 A. S. Fonseca, A.-K. Viitanen, A. J. Koivisto, A. Kangas, M. Huhtiniemi, T. Hussein, E. Vanhala, M. Viana, X. Querol and K. Hämeri, *Ann. Occup. Hyg.*, 2015, **59**, 586–599.
54 B. R'mili, O. L. C. Le Bihan, C. Dutouquet, O. Aguerre-Charriol and E. Frejafon, *Aerosol Sci. Technol.*, 2013, **47**, 767–775.
55 I. Ogura, N. Hashimoto, M. Kotake, H. Sakurai, A. Kishimoto and K. Honda, *Aerosol Sci. Technol.*, 2014, **48**, 758–767.
56 M. E. Birch and R. A. Cary, *Aerosol Sci. Technol.*, 1996, **25**, 221–241.
57 M. E. Birch, *Diesel particulate matter (as elemental carbon) 5040 in NIOSH manual of analytical methods (NMAM)*, The National Institute for Occupational Safety and Health (NIOSH), 4th edn, 2003.
58 M. E. Birch, *Monitoring of diesel particulate exhaust in the workplace in NIOSH manual of analytical methods (NMAM)*, The National Institute for Occupational Safety and Health (NIOSH), 4th edn, 2003.
59 EN 17199-1: 2019, *Workplace exposure —Measurement of dustiness of bulk materials that contain or release respirable NOAA and other respirable particles—Part 1: Requirements and choice of test methods*, CEN, 2019.
60 EN 17199-2:2019, *Workplace exposure—Measurement of dustiness of bulk materials that contain or release respirable NOAA or other respirable particles—Part 2: Rotating drum method*, CEN, 2019.
61 EN 16966:2018, *Workplace exposure—Measurement of exposure by inhalation of nano-objects and their aggregates and agglomerates. Metrics to be used such as number concentration, surface area concentration and mass concentration*, CEN, 2018.
62 EN 17058:2018, *Workplace exposure —Assessment of exposure by inhalation of nano-objects and their aggregates and agglomerates*, CEN, 2018.
63 M. Poikkimäki, V. Koljonen, N. Leskinen, M. Närhi, O. Kangasniemi, O. Kausiala and M. Dal Maso, *Environ. Sci. Technol.*, 2019, **53**, 13618–13628.
64 P. J. Drivas, P. A. Valberg, B. L. Murphy and R. Wilson, *Indoor Air*, 1996, **6**, 271–277.
65 Y.-S. Lee, J.-H. Sung, K.-S. Song, J.-K. Kim, B.-S. Choi, I.-J. Yu and J.-D. Park, *Toxicol. Res.*, 2019, **8**, 580–586.
66 L. Ma-Hock, V. Strauss, S. Treumann, K. Küttler, W. Wohlleben, T. Hofmann, S. Gröters, K. Wiench, B. Van Ravenzwaay and R. Landsiedel, *Part. Fibre Toxicol.*, 2013, **10**, 23.
67 O. Creutzenberg, H. Oliveira, L. Farcal, D. Schaudien, A. Mendes, A. C. Menezes, T. Tischler, S. Burla and C. Ziemann, *Nanomaterials*, 2022, **12**, 1254.
68 J. H. Shin, S. G. Han, J. K. Kim, B. W. Kim, J. H. Hwang, J. S. Lee, J. H. Lee, J. E. Baek, T. G. Kim, K. S. Kim, H. S. Lee, N. W. Song, K. Ahn and I. J. Yu, *Nanotoxicology*, 2015, **9**, 1023–1031.
69 J. K. Kim, J. H. Shin, J. S. Lee, J. H. Hwang, J. H. Lee, J. E. Baek, T. G. Kim, B. W. Kim, J. S. Kim, G. H. Lee, K. Ahn, S. G. Han, D. Bello and I. J. Yu, *Nanotoxicology*, 2016, **10**, 891–901.
70 Y. H. Kim, M. S. Jo, J. K. Kim, J. H. Shin, J. E. Baek, H. S. Park, H. J. An, J. S. Lee, B. W. Kim, H. P. Kim, K. H. Ahn, K. Jeon, S. M. Oh, J. H. Lee, T. Workman, E. M. Faustman and I. J. Yu, *Nanotoxicology*, 2018, **12**, 224–238.
71 S. G. Han, J. K. Kim, J. H. Shin, J. H. Hwang, J. S. Lee, T.-G. Kim, J. H. Lee, G. H. Lee, K. S. Kim, H. S. Lee, N. W. Song, K. Ahn and I. J. Yu, *BioMed Res. Int.*, 2015, **2015**, 1–9.
72 N. Hadrup, N. Sahlgren, N. R. Jacobsen, A. T. Saber, K. S. Hougaard, U. Vogel and K. A. Jensen, *Nanotoxicology*, 2023, **17**, 338–371.
73 *Guidance on information requirements and chemical safety assessment: Part E: risk characterisation*, ed. European Chemicals Agency, ECHA, Helsinki, Version 3.0., 2016.
74 A. Spinazzè, A. Cattaneo, F. Borghi, L. Del Buono, D. Campagnolo, S. Rovelli and D. M. Cavallo, *Int. J. Hyg. Environ. Health*, 2019, **222**, 76–83.
75 F. Pitaro, S. Seeger and B. Nowack, *Environ. Int.*, 2025, **197**, 109345.
76 P. van Broekhuizen, W. van Veelen, W.-H. Streekstra, P. Schulte and L. Reijnders, *Ann. Occup. Hyg.*, 2012, **56**, 515–524.
77 D. H. Brouwer, I. H. M. Links, S. A. F. de Vreede and Y. Christopher, *Ann. Occup. Hyg.*, 2006, **50**, 445–452.
78 I. Ogura, H. Sakurai and M. Gamo, *J. Phys.: Conf. Ser.*, 2009, **170**, 012003.
79 T. Schneider and K. A. Jensen, *Ann. Occup. Hyg.*, 2008, **51**, 23–34.
80 A. R. Murray, E. R. Kisin, A. V. Tkach, N. Yanamala, R. Mercer, S.-H. Young, B. Fadeel, V. E. Kagan and A. A. Shvedova, *Part. Fibre Toxicol.*, 2012, **9**, 10.
81 C. Dazon, S. Bau, R. Payet, V. Fierro and O. Witschger, *Environ. Sci.:Processes Impacts*, 2023, **25**, 670–679.
82 V.-M. Hiltunen, P. Koskinen, K. K. Mentel, J. Manninen, P. Myllyperkiö, M. Pettersson and A. Johansson, *npj 2D Mater. Appl.*, 2021, **5**, 49.
83 J. Aumanen, A. Johansson, J. Koivistoinen, P. Myllyperkiö and M. Pettersson, *Nanoscale*, 2015, **7**, 2851–2855.
84 S. Damilos, D. Semitekolos, S. Saliakas, A. Kostapanou, C. Charitidis and E. P. Koumoulos, *Safety*, 2025, **11**, 11.
85 H. Gao, W. He, R. Yu, T. Hammer, G. Xu and J. Wang, *Sep. Purif. Technol.*, 2020, **251**, 117293.

86 Z. Li, R. J. Young, C. Backes, W. Zhao, X. Zhang, A. A. Zhukov, E. Tillotson, A. P. Conlan, F. Ding, S. J. Haigh, K. S. Novoselov and J. N. Coleman, *ACS Nano*, 2020, **14**, 10976–10985.
87 OECD, *Test No. 412: Subacute Inhalation Toxicity: 28-Day Study*, OECD Publishing, 2018.
88 OECD, *Test No. 413: Subchronic Inhalation Toxicity: 90-Day Study*, OECD Publishing, 2018.
89 J. P. M. Andrews, S. S. Joshi, E. Tzolos, M. B. Syed, H. Cuthbert, L. E. Crica, N. Lozano, E. Okwelogu, J. B. Raftis, L. Bruce, C. A. Poland, R. Duffin, P. H. B. Fokkens, A. J. F. Boere, D. L. A. C. Leseman, I. L. Megson, P. D. Whitfield, K. Ziegler, S. Tammireddy, M. Hadjidemetriou, C. Bussy, F. R. Cassee, D. E. Newby, K. Kostarelos and M. R. Miller, *Nat. Nanotechnol.*, 2024, **19**, 705–714.
90 M. Niang, N. Barcellos, M. Edmondson, L. Chen, S. McCormick and M. M. Dahm, *J. Occup. Environ. Hyg.*, 2025, **22**, 62–77.
91 S. P. B. Sousa, T. Peixoto, R. M. Santos, A. Lopes, M. D. C. Paiva and A. T. Marques, *J. Compos. Sci.*, 2020, **4**, 106.
92 L.-M. Lo, D. Hammond, I. Bartholomew, D. Almaguer, W. A. Heitbrink and J. Topmiller, *In-depth survey report: engineering controls for nano-scale graphene platelets during manufacturing and handling processes*, The National Institute for Occupational Safety and Health (NIOSH), 2011.
93 V. B. Mohan, *C*, 2019, **5**, 36.
94 N. M. Neu-Baker, A. Eastlake and L. Hodson, *Int. J. Environ. Res. Public Health*, 2022, **19**, 7676.
95 T. Kanerva and J. Catalán, Fact sheet: Best practices for safe graphene work, Finnish Institute of Occupational Health, 2023, Available at: https://www.ttl.fi/file-download/download/public/6726 (English), https://www.ttl.fi/file-download/download/public/6725 (Finnish), https://www.ttl.fi/file-download/download/public/6755 (Italian), https://www.ttl.fi/file-download/download/public/6754 (Spanish), Accessed on 3rd April 2025.
96 S. McCormick, M. Niang and M. M. Dahm, *Curr. Environ. Health Rep.*, 2021, **8**, 223–234.
97 M. V. D. Z. Park, E. A. J. Bleeker, W. Brand, F. R. Cassee, M. Van Elk, I. Gosens, W. H. De Jong, J. A. J. Meesters, W. J. G. M. Peijnenburg, J. T. K. Quik, R. J. Vandebriel and A. J. A. M. Sips, *ACS Nano*, 2017, **11**, 9574–9593.
98 P. Nymark, M. Bakker, S. Dekkers, R. Franken, W. Fransman, A. García-Bilbao, D. Greco, M. Gulumian, N. Hadrup, S. Halappanavar, V. Hongisto, K. S. Hougaard, K. A. Jensen, P. Kohonen, A. J. Koivisto, M. Dal Maso, T. Oosterwijk, M. Poikkimäki, I. Rodriguez-Llopis, R. Stierum, J. B. Sørli and R. Grafström, *Small*, 2020, **16**, 1904749.
99 J. D. Ede, A. S. Diges, Y. Zhang and J. A. Shatkin, *NanoImpact*, 2024, **33**, 100488.
100 European Commission: Joint Research Centre, *Safe and sustainable by design chemicals and materials: review of safety and sustainability dimensions, aspects, methods, indicators, and tools,* Publications Office of the European Union, 2022.